Enantioselective membranes prepared by electrospinning of cellulose tris(3,5-dimethylphenyl carbamate) having various degrees of polymerization: effect of the DP on the morphology

Steve Nono-Tagne, Yotam Navon, Yu Ogawa, Bruno Carré, Issei Otsuka

Preprint (submitted version) of the manuscript in *Cellulose* (2024) 31:2765–2782. DOI:10.1007/s10570-023-05644-4

Enantioselective membranes prepared by electrospinning of cellulose tris-(3,5-dimethylphenylcarbamate) synthesized from hardwood cellulose fibers

Steve Nono-Tagne,[a] Yotam Navon,[b] Yu Ogawa,[a] Bruno Carré,[b] and Issei Otsuka[a*]

[a] *Univ. Grenoble Alpes, CNRS, CERMAV, Grenoble 38000, France*

[b] *Centre Technique du Papier, Grenoble 38044, France*

*Corresponding author: I. Otsuka

E-mail address: issei.otsuka@cermav.cnrs.fr
ORCID: 0000-0002-9049-7350

Abstract: Cellulose phenyl carbamates such as cellulose tris-(3,5-dimethyl phenyl carbamate) (CDMPC) are known to act as chiral selectors when they are immobilized on silica gels that are packed in the columns for high-performance liquid chromatography (HPLC). Previously, we reported a proof of concept of enantioselective membrane filtration using a nonwoven membrane prepared by electrospinning of the CDMPC synthesized from microcrystalline cellulose Avicel®. In the present work, TECHNOCEL® cellulose fiber samples derived from hardwood are functionalized to synthesize CDMPCs having higher and different degrees of polymerizations. The length and width of the cellulose fiber samples are characterized using a MorFi image analyzer. The obtained CDMPCs are electrospun to form nanofibrous membranes and their morphology is studied in relation to the electrospinning process parameters, the degrees of polymerizations of the CDMPCs, and their solution concentrations. Liquid-liquid permeation experiments of a racemic compound, (*R*,*S*)-1-(1-naphthyl)ethanol, through the CDMPCs membranes demonstrate preferable permeation of the *S*-enantiomer. This is supported by theoretical simulations using a molecular docking model that indicate stronger hydrogen bonding and π-π interactions with higher binding energy between CDMPC and the *R*-enantiomer than the *S*-enantiomer.

Keywords: Cellulose tris-(3,5-dimethyl phenyl carbamate), Electrospinning, Nanofiber, Enantioselective membrane, Chiral resolution, Molecular docking simulation

Introduction

Biologically active compounds, such as drugs, agrochemicals, food additives, etc. often contain chiral structures in their molecules. Since their physiological properties usually depend on this chirality, great efforts have been made to produce chirally pure compounds. In general, there are two typical approaches (Kaya et al. 2023): one is asymmetric synthesis and the other is chiral resolution, in most cases, by High Performance Liquid Chromatography (HPLC) (Okamoto and Ikai 2008; Shen and Okamoto 2016). The former uses chiral sources such as chiral catalysts and enzymes that are often specific for each desired chiral molecule and is, thus, not a versatile approach for various chiral compounds despite its potential for large-scale production. On the other hand, the latter is more versatile for producing various chiral compounds although it is unsuitable for large-scale production due to its discontinuous batch process. We note that the chiral chemicals market size is expected to increase by 5.89 billion US$ from 2020 to 2025 according to TechNavio Ltd., UK ("Chiral Chemicals Market by Application and Geography - Forecast and Analysis 2021-2025" https://www.technavio.com/report/chiral-chemicals-market-industry-analysis. Accessed on February 16, 2023). Given this rapid expansion, there is urgent need for novel strategies that enable large-scale continuous chiral resolution based on a deeper understanding of the mechanism.

Chiral resolution via enantioselective membrane filtration, which is one of the promising strategies for large-scale continuous processing, has been reported since 1980s (Liu et al. 2021; Vedovello et al. 2022). Various enantioselective membranes were prepared from natural chiral polymers (e.g., polypeptides and polysaccharides) and their derivatives. Aiming to improve the interaction between the membranes and chiral molecules, porous materials with large specific surface area (SSA) such as metal organic frameworks (MOFs) (Das et al. 2018; Gong et al. 2022) and covalent organic frameworks (COFs) (Wang et al. 2020; Zhuo et al. 2020) were recently utilized as ingredients of enantioselective membranes. Electrospun nanofibrous textile is another potential material of enantioselective membranes with large SSA and mechanical integrity. For example, chemically and/or physically functionalized achiral synthetic polymers such as poly(ethylene terephthalate) (Yoshimatsu et al. 2008) and polysulfone (Mizushima et al. 2012; Sueyoshi et al. 2012; Yoshikawa et al. 2007) with various chiral selectors (CSs) were electrospun to form nanofibrous membranes and their potential for chiral resolutions have been reported. Electrospun membranes made of polysaccharides such as cellulose triacetate (Kawasaki and Yoshikawa 2013) and chitin (Shiomi and Yoshikawa 2013; Shiomi and Yoshikawa 2016) and their derivatives also demonstrated chiral resolution properties. Although these previous and cutting-edge studies ensure a promising outlook of the membrane-based chiral resolutions, there are still many hurdles to overcome for efficient chiral resolutions as has been achieved by HPLC. In addition, the detailed mechanism of chiral discrimination at a molecular level is still unclear.

Polysaccharides and their derivatives have been widely used as CSs in chiral resolutions (Okamoto and Yashima 1998; Peluso et al. 2020). Among them, cellulose and amylose derivatives notably phenylcarbamates and esters are known as the most popular CSs when immobilized on silica gels, so-called chiral stationary phases (CSPs), that are packed in the columns for HPLC.

Despite their discrimination properties for a wide range of chiral molecules, these polysaccharide based CSs always need a kind of scaffold to be immobilized, e.g., silica gels in the case of CSPs in HPLC columns. Recently, we prepared a self-standing nanofibrous membrane made of cellulose tris(3,5-dimethylphenylcarbamate) (CDMPC), one of the most versatile CSs used in chiral HPLC columns, by electrospinning and demonstrated their enantioselective permeation property (Otsuka et al. 2021). The great advantage of electrospinning is that one can prepare the enantioselective membrane consisting purely of the CS, in this case CDMPC, as the spinning polymer. In addition, thanks to their simple fabrication process, the morphology of electrospun membranes can be controlled. Indeed, important properties of the nanofibrous membranes such as the fiber diameter, membrane thickness, porosity, SSA etc. can be controlled by adjusting the process parameters (e.g., applied voltage, solution feed rate, and tip-to-collector distance) (Thompson et al. 2007) as well as the properties of the spinning polymer (e.g. degree of polymerization (DP), solvent, and concentration) (Fong et al. 1999; Greiner and Wendorff 2007).

In this study, CDMPCs having different DPs are synthesized from hardwood-derived cellulose fiber samples with different fiber length and width. The CDMPCs are electrospun and the morphologies of the products are investigated with variation of the process parameters such as the applied voltage and the solution feed rate, as well as the DPs and the concentrations of the CDMPCs. Enantioselective permeation of (*R*,*S*)-1-(1-naphthyl)-ethanol through the electrospun membranes is characterized by liquid-liquid permeation experiments. Molecular binding free energies between CDMPC and *R*-/*S*-1-(1-naphthyl)ethanol are theoretically calculated by a molecular docking method and compared to the experimental results of the enantioselective permeation.

Experimental

Materials

TECHNOCEL®-10, -200, and -1000 cellulose fiber samples were gifted from CFF GmbH & Co. and used after drying under vacuum at 65 °C overnight. 3,5-Dimethyl phenyl isocyanate (99%) was purchased from Alfa Aesar Co. and used as received. (*R*,*S*)-1-(1-naphthyl)ethanol (≥ 99.0%), *n*-hexane for HPLC (≥ 95%), 2-propanol gradient grade for liquid chromatography (≥ 99.9%), and *N*,*N*-dimethylacetamide (DMAc) (99%) were purchased from Sigma-Aldrich Co. and used as received. Acetone (≥ 99.8%), dimethylformamide (DMF), tetrahydrofuran (THF), and ethanol were purchased from Biosolve Chimie Co. and used as received. Methanol (≥ 99%) was purchased from Carlo Erba Co. and used as received.

Instruments

Attenuated Total Reflection-Fourier Transform Infrared (ATR-FTIR) spectra were obtained using a PerkinElmer Spectrum Two spectrometer. Proton nuclear magnetic resonance (^{1}H NMR) spectra

were recorded on a Bruker Advance DRX400 (400 MHz) spectrometer. Size Exclusion Chromatography (SEC) was performed with an Agilent Technologies 1260 Infinity Multi Detector Suite GPC/SEC System equipped with a refractive index (RI) detector, a ultraviolet (UV) detector, and a dual-angle (90° and 15°) light scattering (LS) detector, and a set of columns (Shodex Asahipak GF-1G 7B, GF-7M HQ, and GF-310 HQ) operating at 40 °C using DMF containing 0.01 M LiCl as an eluent at a flow rate of 0.6 mL/min. A Wyatt Optilab rEx differential refractive index detector was used to determine dn/dc values. Electrospinning was performed by a Fuence Esprayer ES-2000S2A. The scanning electron microscope (SEM) images of the specimens coated with a ca. 4 nm-thick layer of gold/palladium (Au/Pd) were observed by a FEI QUANTA FEG 250 microscope operating at an accelerating voltage of 2.5 kV. High Performance Liquid Chromatography (HPLC) was performed with a Thermo Fisher Scientific UltiMate 3000 HPLC system equipped with a VWD-3100 UV (λ = 270 nm) detector and a Daicel CHIRALPAK® IB N-3 (length × inner diameter: 100 × 4.6 mm, particle size: 3 μm) analytical column operating at 30 °C using a mixed solvent of *n*-hexane and 2-propanol, i.e. *n*-hexane/2-propanol = 9/1 (v/v), as an eluent at a flow rate of 1.0 mL/min. A Techpap MorFi image analyzer was used to characterize TECHNOCEL cellulose fibers' morphology by image analysis.

Morphological characterization of TECHNOCEL cellulose fiber samples

0,3 g of each TECHNOCEL fiber sample was dispersed in 1 L of water and characterized with the MorFi image analyzer. Several thousand fibers were analyzed in order to assess cellulosic fiber dimensions: average and distribution of fibers lengths and widths. The mean fiber lengths (mean length-weighted length) were determined as below:

$$\sum_{i=1}^{n}(L_i \times L_i) \Big/ \sum_{i=1}^{n} L_i$$

where L_i is the length of the fiber i.

Syntheses of CDMPCs

Syntheses of CDMPCs from TECHNOCEL cellulose fiber samples were achieved according to a previously reported method used for microcrystalline cellulose as the starting material (Okamoto et al. 1986) with several modifications. TECHNOCEL-10, -200, and -1000 samples (1.00 g of each) were vigorously stirred in dry pyridine under reflux until the fibers disperse completely without any aggregation: TECHNOCEL-10 and -200 were stirred in 25 mL of pyridine for 12 h, while TECHNOCEL-1000 was stirred in 50 mL of pyridine for 24 h. After cooling down the suspensions to room temperature, an excess of 3,5-dimethylphenyl isocyanate (5.00 g, 34.0 mmol) were added dropwise to the suspensions and the mixtures were stirred under reflux for 24 h for the mixture of TECHNOCEL-10 and 48 h for those of TECHNOCEL-200 and -1000. The mixtures were cooled to room temperature, then slowly poured into methanol. The precipitates were collected by filtration, then dissolved in THF and re-precipitated in methanol. Finally, the

precipitates collected by filtration were dried in vacuo to obtain CDMPC-10, -200, and -1000 (the numbers are corresponding to those of the starting TECHNOCEL samples) as white solids (yields: 3.26 g, 3.23 g, and 3.04 g for CDMPC-10, -200, and -1000, respectively). The molecular weights and molecular weight distributions were determined by SEC analysis and summarized in Table 1. The degree of substitution (DS) of the CDMPCs were calculated from the ^{1}H NMR spectra according to the following equation:

$$\mathrm{DS} = \frac{\sum \mathrm{H_{AGU}} \cdot \int \mathrm{H_{N\mathit{H}}}}{\int \mathrm{H_{AGU}} \cdot \sum \mathrm{H_{N\mathit{H}}}}$$

where $\sum \mathrm{H_{AGU}}$ is 7 protons in the anhydroglucose unit (AGU), $\sum \mathrm{H_{N\mathit{H}}}$ is 1 proton of N-*H* in the urethane group, $\int \mathrm{H_{AGU}}$ is integral of the 7 protons in the AGU, and $\int \mathrm{H_{N\mathit{H}}}$ is integral of the 1 proton of N-*H* in the urethane group.

Electrospinning

The electrospinnings of the CDMPCs (0.82 g for all the samples) dissolved in a mixed solvent system, acetone/DMF = 3/2 (v/v), with various concentrations (2-12 wt%) were performed at room temperature (ca. 25 °C) and humidity (ca. 30%). A metallic electrode plate (20 cm × 20 cm square) covered with aluminum foil was placed at 15 cm below the tip of the needle (Nordson stainless steel tips 18 gauge; inner diameter = 0.84 mm, outer diameter = 1.27 mm). A high voltage of 15 kV (unless stated otherwise) was applied between the needle and the electrode plate while the sample solutions were passed with an appropriate solution feed rate 10 μL/min (unless stated otherwise) from the needle to the collector. The electrode plate was continuously moved as its center draws a 5 cm × 5 cm square controlled by a computer program so that the fibers are electrospun evenly over the entire surface of the aluminum foil.

Morphological characterization of the electrospun products

The morphology of the electrospun products was characterized by SEM observation. The diameters of the electrospun fibers in the membranes and their distributions were statistically analyzed utilizing more than 100 randomly selected fibers from the SEM images using ImageJ open-source software. It should be noted that several SEM images were used for the statistical analysis when there was a small number of the fibers in one image. The thicknesses of the membranes were measured using a Mitutoyo IP65 Digital Micrometer. The specific surface areas (SSAs) of the CDMPCs membranes were determined by measuring adsorption-desorption isotherms of nitrogen at 77 K using a Micromeritics ASAP 2010 volumetric apparatus as described in the literature (Fumagalli et al. 2013).

Chiral separation

Chiral separation of (*R*,*S*)-1-(1-naphthyl)-ethanol as a model racemic compound was performed via liquid-liquid permeation (Otsuka et al. 2021) as detailed below. An electrospun CDMPC membrane collected on an aluminum foil was cut into a small piece (ca. 3 cm × 3 cm square) and the membrane was carefully peeled off from the aluminum foil using tweezers. The peeled membrane was sandwiched between two Whatman® polytetrafluoroethylene (PTFE) membrane filters (pore size: 1 μm, diameter: 47 mm) as a support of the membrane to compose the final CDMPC membrane system. The CDMPC membrane system was arranged between a pair of 15 mm unjacketed "Side-Bi-Side" glass cells (PermeGear Inc.) equipped with magnetic stir bars in each cell. A mixed solvent of *n*-hexane and 2-propanol) with the volume ratio of 9 to 1 (*n*-hexane/2-propanol = 9/1 (v/v)) was used as eluent for the following permeation experiments (cf. Figure 8). A 5 mL solution of (*R*,*S*)-1-(1-naphthyl)-ethanol in the eluent (2 g/L) was placed in the left-side cell and a 5 mL of the eluent was placed in the right-side cell. The solutions in both cells were stirred and a 150 μL of the solution in the right-side cell was sampled every 1 minute for the HPLC analysis. The sample solutions containing permeated *R*- and *S*-1-(1-naphthyl)-ethanol from the right-side cell were analyzed by the HPLC equipped with a CDMPC packed column (Daicel CHIRALPAK® IB N-3). The enantiomeric excess (*e.e.*) values (%) of the samples were determined by comparing the two independent peak areas of the *S*-enantiomer and the *R*-enantiomer from the HPLC chromatograms according to the following equation:

$$e.e.(\%) = \frac{\mathrm{A_S} - \mathrm{A_R}}{\mathrm{A_S} + \mathrm{A_R}} \times 100$$

where A_S and A_R are the peak areas of the *S*-enantiomer and the *R*-enantiomer in the chromatogram, respectively.

Water contact angle (WCA) measurement

The WCAs of the CDMPCs membranes were examined using an I.T. Concept Tracker tensiometer at room temperature. A 10 μL of deionized water was dropped on each membrane fixed on a glass slide and the contact angle was measured when the angle became stable after 15 sec. Measurements were made five times for each membrane and the mean angle was determined as the WCA for each sample.

Molecular construction and docking simulation

ChemBioDraw Ultra version 12.0 (PerkinElmer Inc.) was used to construct the 3D structures of CDMPC, *R*-1-(1-naphthyl)ethanol, and *S*-1-(1-naphthyl)ethanol. The structures were then energy minimized using the MM2 energy minimization algorithm of ChemBio3D. AutoDock version 4.2 (Scripps Research Institute), PyMOL version 1.5.7 (Schrödinger, Inc.), and BIOVIA Discovery studio visualizer 4.5 (3DEXPERIENCE) open-source software were used for docking simulations. AutoDock Tools (ADT) 1.5.6. was employed to process the structures of CDMPC, *R*-1-(1-naphthyl)ethanol, and *S*-1-(1-naphthyl)ethanol prior to docking. For CDMPC, the Kollman and Gasteiger charges were computed, while for *R*- and *S*-1-(1-naphthyl)ethanol, Gasteiger charges

and rotatable bonds were assigned. The structures of *R*- and *S*-1-(1-naphthyl)ethanol (Ligands) were treated as flexible while the structure of CDMPC was kept rigid in the docking protocol. The AutoGrid program was employed to generate 3D affinity grid fields. A grid of size ca. 80×70×40 $Å^3$ with 0.375 Å spacing was used for docking. The default settings were used for all other parameters. CDMPC–Ligands interactions and scoring functions were used to choose the docked structures and for further analysis. Results differing by less than 2 Å in a positional all atom-based root mean-square deviation (RMSD) were clustered together. The average binding free energy was calculated according to the following equation (Ke et al. 2021; Luo et al. 2022):

$$E = \sum_{i=1}^{n} (E_i \times X_i)$$

where E is the average binding free energy, n is the number of conformational clusters, E_i is the binding free energy of this cluster conformation, X_i is percentage frequency of this cluster conformation. The greater negative values of the binding energy reflect the greater stability of the enantiomer–CDMPC binding.

Results and discussion

Synthesis of CDMPCs having different DPs

A variety of cellulose triphenylcarbamate derivatives were synthesized from commercially available microcrystalline cellulose and their properties as CSs for enantioseparation have been widely studied. In most cases, the CSs were immobilized on silica gels to be packed in HPLC columns and used as CSPs. Recently, we discovered a new potential of a representative CS, CDMPC, as enantioselective membranes in the form of electrospun nonwoven textiles. The molecular weight is one of the important parameters governing the morphology of the membranes, which must be investigated in relation to the electrospinning process parameters to improve the quality of the membranes. For this purpose, CDMPCs having different DPs were synthesized from hardwood derived cellulose fiber samples with different fiber lengths and widths, namely TECHNOCEL-10, -200, and -1000. First, the TECHNOCEL samples were characterized by microscopy and the MorFi image analyzer. Figure 1 shows optical microscope and SEM images of the TECHNOCEL samples. Obviously, the fiber lengths increase with the numerical order of the TECHNOCEL samples, while the fiber widths are almost same. Indeed, the calculated mean fiber lengths of TECHNOCEL-10, -200, and -1000 were 305.0 μm, 398.5 μm, and 617.5 μm, respectively, and the distributions (%) of short fibers decreased, while those of long fibers increased with the numerical order of the TECHNOCEL samples as shown in the top of Figure 2. On the other hand, the calculated mean fiber widths are around 20 μm for all the TECHNOCEL samples and the distributions of the fiber widths were almost same as shown in the bottom of Figure 2.

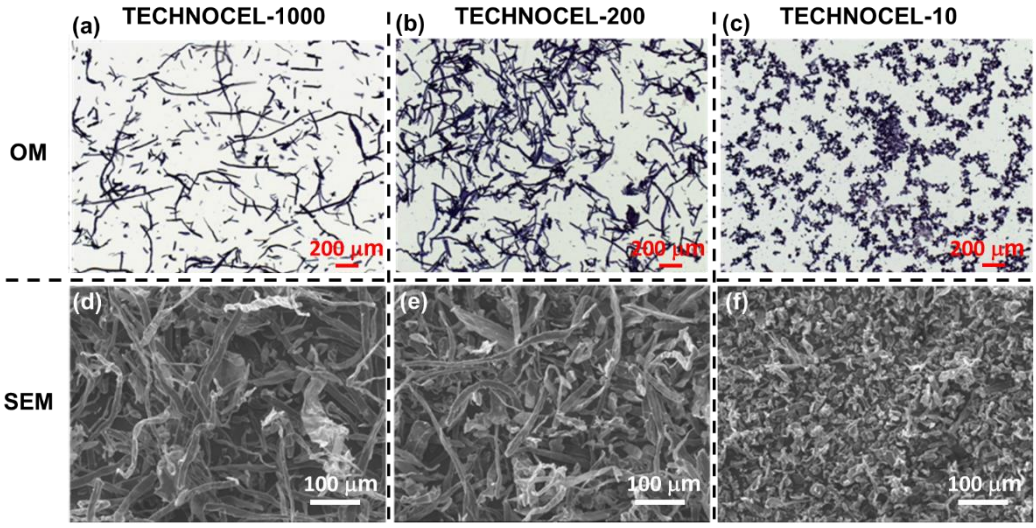

Figure 1. Optical microscope (OM) images (top) and SEM images (bottom) of TECHNOCEL-1000 (a and d), -200 (b and e), and -10 (c and d).

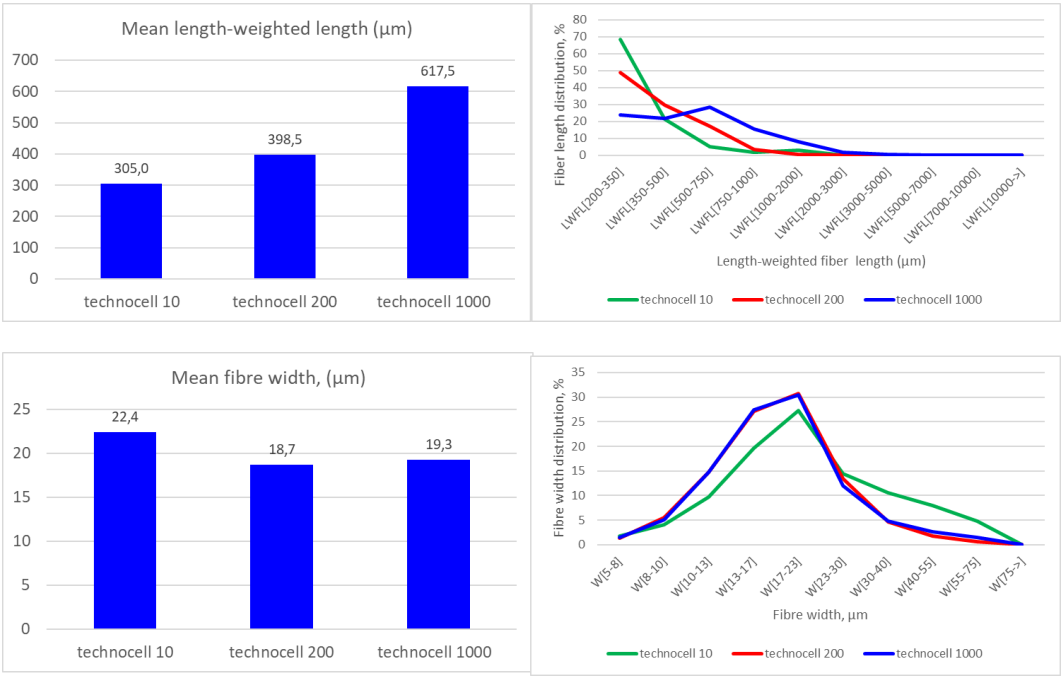

Figure 2. The mean fiber lengths and fiber lengths distribution (top) and the fiber widths and fiber widths distributions (bottom) of TECHNOCEL-10, -200, and -1000 determined by the MorFi analyses.

Second, the TECHNOCEL samples were functionalized with 3,5-dimethylphenyl isocyanate in pyridine to synthesize the CDMPCs using a reported method (Okamoto et al. 1986) for the functionalization of microcrystalline cellulose with several modifications (Scheme 1). For successful functionalization, it was important to pre-disperse the TECHNOCEL samples in pyridine by vigorously stirring them under reflux before starting the reactions in order to avoid

aggregation of the cellulose fibers that hinder the reactions. As the reactions proceeded, the mixtures became homogeneous solutions and the products were isolated by re-precipitations of the mixtures from THF to methanol. Figure 2 shows ATR-FTIR spectra of the starting cellulose samples (TECHNOCEL-10, -200, and -1000) and the corresponding functionalized products (namely CDMPC-10, -200, and -1000). In the spectra of the TECHNOCEL samples (the spectra shown in black), typical broad absorption bands corresponding to the O-H stretching vibration of cellulose were observed in 3600–3000 cm^{-1} region. On the other hand, these broad absorption bands of the hydroxyl groups of cellulose did not exist in the spectra of the functionalized products (the spectra shown in red), while absorption bands corresponding to the N-H stretching vibration around 3475 cm^{-1}, the C=O stretching vibration around 1715 cm^{-1}, and the C-C stretching vibration in the aromatic ring around 1590 cm^{-1}, 1520 cm^{-1}, and 1445 cm^{-1} were clearly observed. ^{1}H NMR spectra of the products shown in Figure 4 demonstrate characteristic signals of urethane N-H protons (8.6-8.0 ppm), aromatic protons (7.4–6.2 ppm), cellulose backbone protons (5.2–3.4 ppm), and aryl-methyl protons (2.5–1.7 ppm) corresponding to the chemical structure of CDMPC. The DS values calculated from the peak integrations of the N-H protons and the cellulose backbone protons were almost 3 (the calculated DS values for CDMPC-10, -200, and -1000 were 3.08, 3.15, and 3.01), which confirms quantitative substitutions of the hydroxyl groups on the starting cellulose by 3,5-dimethylphenyl carbamate groups. These results are in line with that reported in literature for the CDMPCs synthesized from microcrystalline cellulose (Bui et al. 2023; Otsuka et al. 2021; Weng et al. 2013). Absolute molecular weights of the CDMPCs were measured by SEC equipped with a dual-angle (15° and 90°) LS detector. The SEC traces (intensity of LS at 15° vs. elution time) of the CDMPCs and a CDMPC synthesized from microcrystalline cellulose (CDMPC-MCC) previously reported by us (Otsuka et al. 2021) for comparison are shown in Figure 5. The number-average molecular weight (M_n), the weight-average molecular weight (M_w), the molecular weight dispersity ($Đ_M = M_w/M_n$), and the DP are summarized in Table 1. All the CDMPCs synthesized from the TECHNOCELs have higher molecular weights than those of CDMPC-MCC and different from each other, i.e., the molecular weights increase in the order of CDMPC-MCC, -10, -200, and -1000. Consequently, the CDMPCs having different DPs were successfully obtained from the TECHNOCEL cellulose fiber samples.

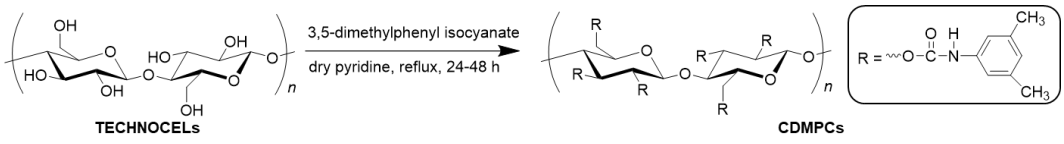

Scheme 1. Synthesis of the CDMPCs from TECHNOCEL hardwood cellulose fiber samples.

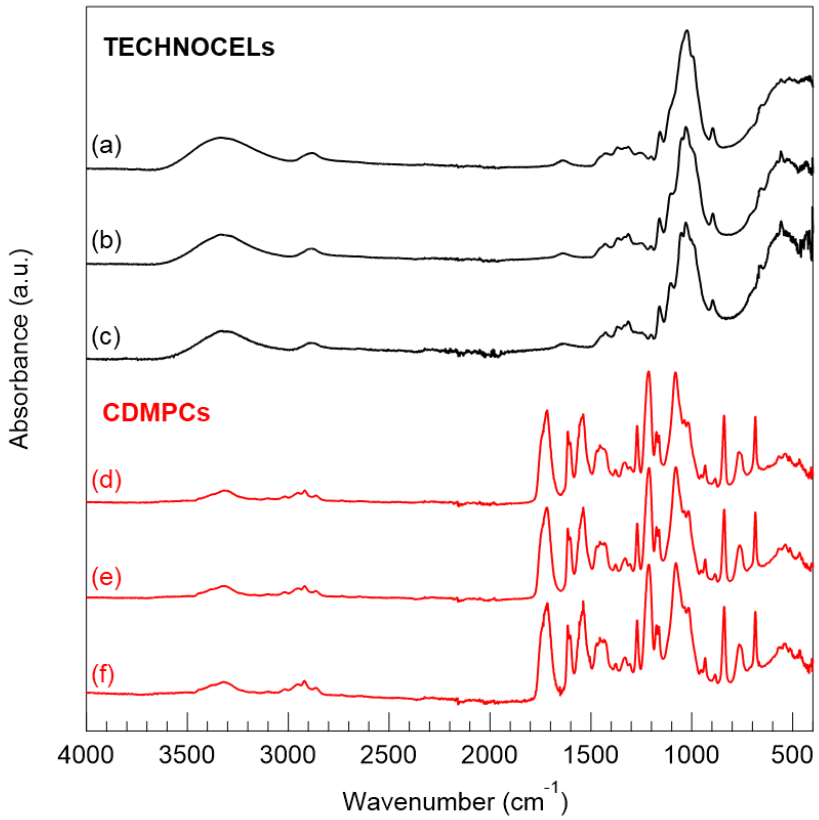

Figure 3. ATR-FTIR spectra of the starting cellulose samples: the spectra (a), (b), and (c) shown in black are respectively TECHNOCEL-10, -200, and -1000, and the products after functionalizations: the spectra (d), (e), and (f) shown in red are respectively CDMPC-10, -200, and -1000.

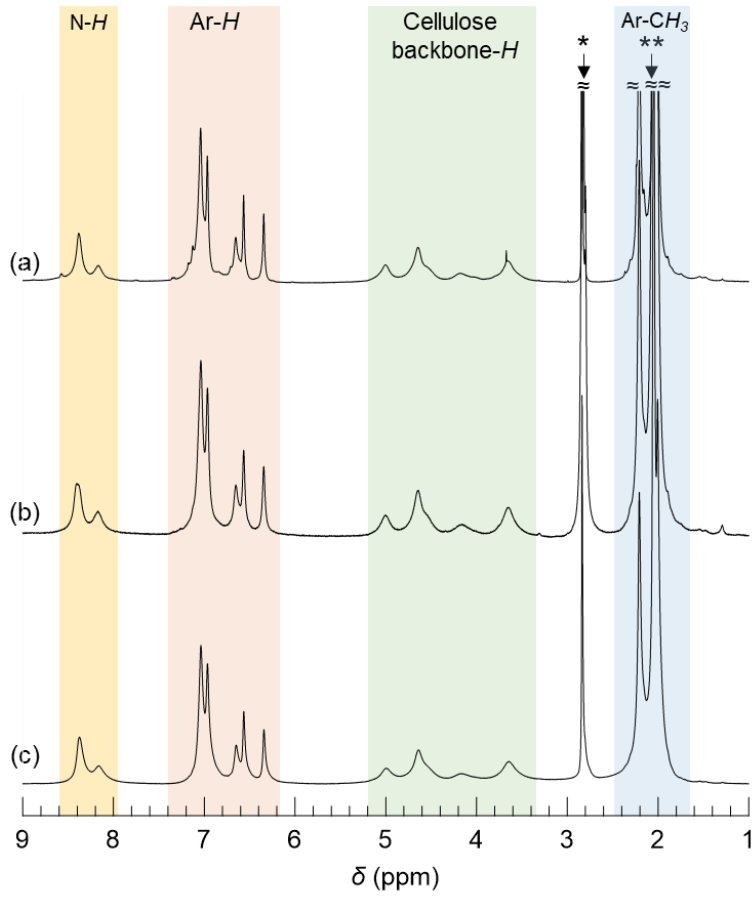

311

312 **Figure 4.** ^{1}H NMR spectra of (a) CDMPC-10, (b) CDMPC-200, and (c) CDMPC-1000 in acetone-
313 d_6 (solvent residual signals: *H_2O and **acetone).

314

315

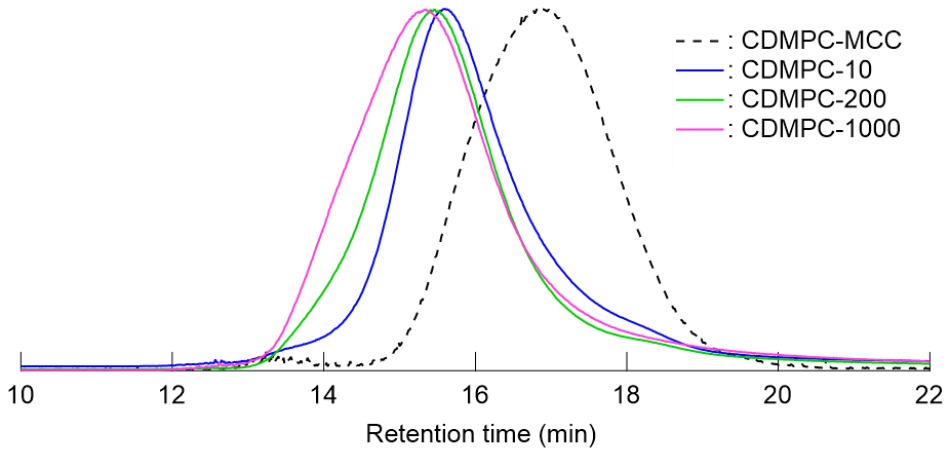

316

317 **Figure 5.** SEC traces of (a) CDMPC synthesized from MCC (CDMPC-MCC) shown with the dot-
318 line, (b) CDMPC-10 shown with the green line, (c) CDMPC-200 shown with the red line, and (d)
319 CDMPC-1000 shown with the blue line.

320

Table 1. Molecular property of the CDMPCs

Starting cellulose	CDMPCs	M_n (g/mol)	M_w (g/mol)	$Đ_M$[a]	DP[b]
MCC (Avicel PH-101)	CDMPC-MCC[c]	87,400	146,000	1.67	242
TECHNOCEL-10	CDMPC-10	399,000	657,000	1.65	1,090
TECHNOCEL-200	CDMPC-200	442,000	895,000	2.02	1,480
TECHNOCEL-1000	CDMPC-1000	609,000	1,170,000	1.93	1,940

[a] $Đ_M = M_w / M_n$. [b] DP = M_w / 603.67: molar mass of the monosaccharide unit of CDMPC (DS = 3).
[c] This polymer was previously reported by the authors (Otsuka et al. 2021).

Electrospinning

The obtained CDMPCs from TECHNOCELs were soluble in several organic solvents that are good solvents of CDMPC-MCC such as acetone, THF, DMF, and DMAc regardless of their DPs. For the successful electrospinning of CDMPC-MCC, it was important to adjust the vapor pressure of the solution by mixing higher volatile solvents (acetone or THF) and lower volatile solvents (DMF or DMAc) in order to stabilize the jet of the solution on the tip of the needle-electrode. Indeed, electrospinning of the solution of CDMPC-MCC in a mixture of higher volatile acetone and lower volatile DMAc with the ratio of 1/1 (v/v) gave a stable electrospinning process to form self-standing nanofibrous membranes. The same solvent system (acetone/DMAc = 1/1 (v/v)), however, did not give good electrospinning condition for the CDMPCs having higher DPs (CDMPC-200 and -1000), i.e. the solvent was not fully evaporated during the elecrospinning process and the collected fibers on the aluminium foil seemed like melted off. Therefore, to improve the volatility, DMAc (bp 165 °C) was replaced by slightly more volatile DMF (bp 153 °C) and the volume ratio of higher volatile acetone (bp 56 °C) was increased from 50% to 60%, i.e., acetone/DMF = 3/2 (v/v). This mixed solvent was adopted as the solvent system for all the electrospinning in this study. Effects of technical parameters such as polymer solution feed rate and applied voltage on the morphology of the electrospun products were investigated as described in the Electronic Supplementary Material.

The morphology of electrospun products is strongly affected by molecular weight (or equivalently, DP) and concentration of polymer that govern the viscosity of the polymer solution. Therefore, various solutions of the CDMPCs having different DPs and concentrations were electrospun with a constant solution feed rate (10 μL/min) and applied voltage (15 kV), and their morphology was characterized by SEM observation. First, CDMPC-10 solutions with the concentrations varied from 2 to 12 wt% in steps of 2% were prepared for the electrospinning. SEM images of the obtained products and the histograms of the constituent fiber diameter distributions determined by statistical analysis of the SEM images are shown in Figure 4. From the solution with the lowest concentration of 2 wt%, fibers coexisting with spherical beads, so-called “bead-on-string” fibers, were obtained (Figure 6a), suggesting that the viscosity and/or surface tension of the solution at this concentration is insufficient against the applied electrostatic force. The increase in polymer concentration to 4 wt% and above led to formations of continuous fibers as shown in

Figure 6b-f. As widely observed in electorspinning of polymer solutions (Ahmadi-Nohadani et al. 2022; Lee et al. 2018; Motamedi et al. 2017), increasing the concentration tended to an increase in mean fiber diameter (MD) from 238 nm (4 wt%) to 554 nm (12 wt%). This can be explained by increase in the viscosity with increase in the solution concentration, i.e., the higher the concentration, the higher the entanglement of the polymer chains, reading them more resistant to the elongation force of the electric field. At the same time, the fiber diameter distributions exhibited a broadening with increasing the concentration, i.e., the standard deviation (SD) value increased from 54 nm (4 wt%) to 137 nm (12 wt%) as shown in Figure 6h-l. This is probably because the electrospinning technical parameters set for the process, such as the distance between the electrodes, the solution feed rate, and the applied voltage kept at constant values were not optimal to allow stable stretching of the polymer solution at higher concentrations. This is especially notable at 12 wt% that shows the most broadened fiber diameter distribution (Figure 6l). It was not possible to electrospin the solution of CDMPC-10 with the concentration beyond 12 wt% due to coagulation of the polymer on the tip of the needle-electrode. The same trend between the polymer concentration and the fiber morphology was observed for CDMPC-200 and CDMPC-1000 as shown in Figure S3 and S4 (in the Electronic Supplementary Material). For all the CDMPCs, the MDs tended to increase with increasing the solution concentrations. The largest SDs were observed at the maximum polymer solution concentrations (12 wt% for CDMPC-10, 8 wt% for CDMPC-200, and 4 wt% for CDMPC-1000) above which the polymers were not electrospinnable due to coagulations of the polymers. It was observed that the maximum concentration decreases as the DP increases as shown in Figure 7. This can be explained by the increase in the viscosity with the increase in the DP, i.e., the higher the DP the more entangled the molecular chains are. In addition, at the same concentration, the MD of the CDMPC having higher DP is always larger compared to the MD with lower DP. For instance, at 4 wt%, the largest MD (993 nm) was observed with CDMPC-1000 (DP = 1,940), followed by the middle MD (539 nm) with CDMPC-200 (DP = 1,480), and the smallest MD (238 nm) with CDMPC-10 (DP = 1,090).

Through the electrospinnings described above, a series of nonwoven nanofibrous membranes consisting of the CDMPCs were formed on aluminum foils that covered the electrode plate. In this study, the total mass of the CDMPCs used for 1 electrospinning process was kept constant (0.82 g) regardless of their solution concentrations. As the morphologies of the electrospun fibers (e.g., diameter, density, and porosity) are different from each other, the thicknesses of the obtained membranes are also different. For this reason, it was not possible to peel off some of the membranes from the aluminum foils due to their thin thickness. The electrospun membranes from the solutions of CDMPC-10 (8, 10, and 12 wt%) and CDMPC-200 (6 and 8 wt%) were successfully peeled off from the aluminum foils. These self-standing membranes (Membrane 1-5 listed in Table 2) were used for the following characterization of enantioselective permeation.

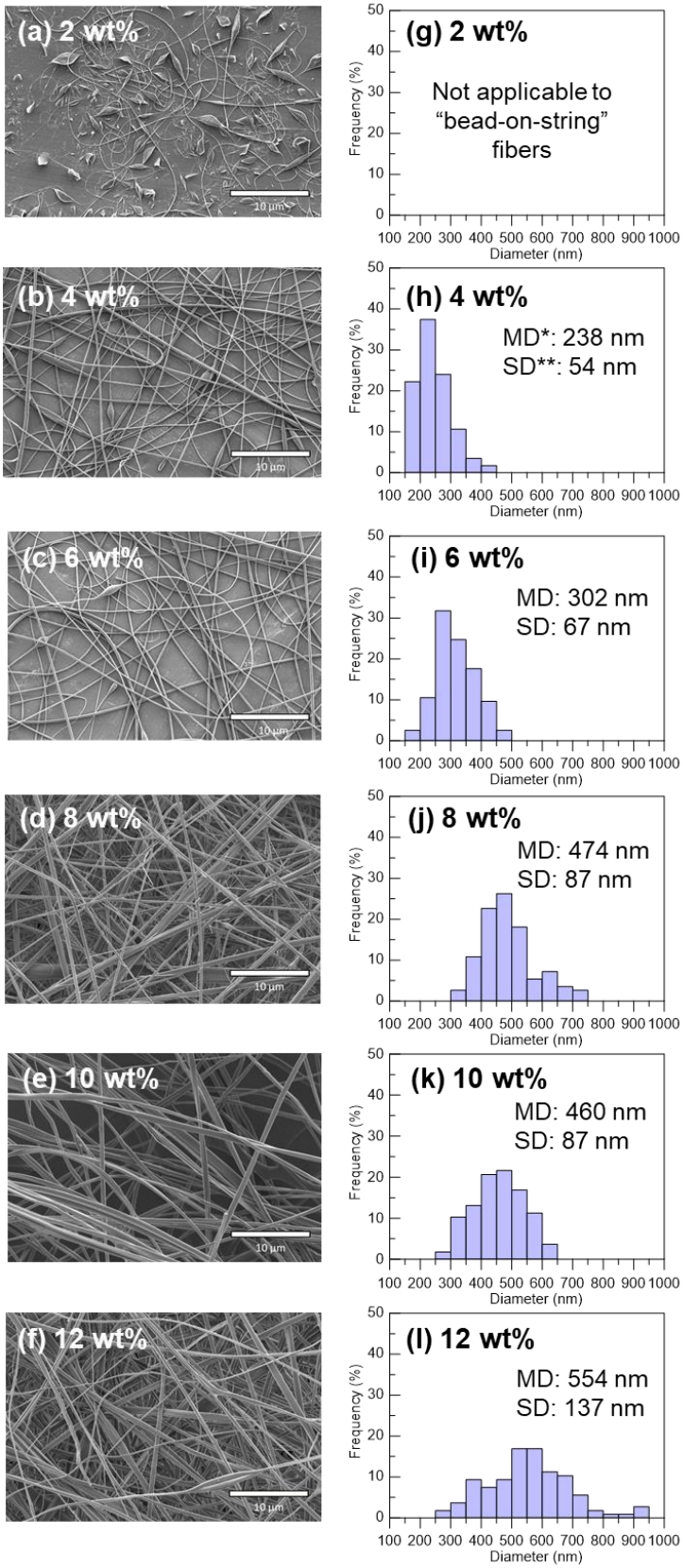

391

392 **Figure 6**. SEM images of the electospun products obtained from the CDMPC-10 solutions in
393 acetone/DMF = 3/2 (v/v) with various concentrations (a-f) and histograms of diameter
394 distributions of the fibers (g-l) determined from the SEM images. *MD: mean diameter. **SD:
395 standard deviation.

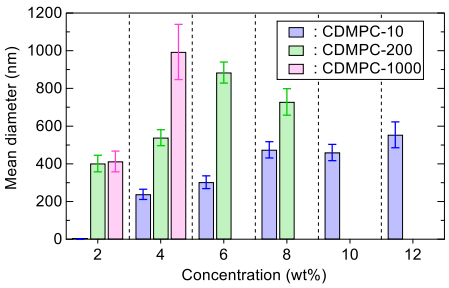

Figure 7. The mean fiber diameters with the standard deviations of the electrospun fibers obtained from CDMPC-10 (the blue bars), CDMPC-200 (the green bars), and CDMPC-1000 (the red bars) solutions with different concentrations.

Table 2. Physical properties of the membranes used for the liquid-liquid permeation experiments

Membrane name	Spinning solution	Thickness (nm)	SSA[a] (m^2/g)	WCA (deg)
Membrane-1	CDMPC-10 (8 wt%)	134	6.8	109.4
Membrane-2	CDMPC-10 (10 wt%)	116	6.0	120.4
Membrane-3	CDMPC-10 (12 wt%)	98	4.7	120.2
Membrane-4	CDMPC-200 (6 wt%)	104	4.1	118.8
Membrane-5	CDMPC-200 (8 wt%)	101	4.2	123.9

[a] Specific surface area was calculated by nitrogen adsorption at 77 K using the BET equation (Brunauer et al. 1938).

Enantioselective permeation of (*R*,*S*)-1-(1-naphthyl)ethanol through the CDMPCs membranes

Previously, we reported the enantioselective permeation of (*R*,*S*)-1-(1-naphthyl)ethanol through the electrospun membrane made of CDMPC-MCC (Otsuka et al. 2021). The preferential adsorption of the *R*-enantiomer into the membrane was a driving force for the preferential permeation of the *S*-enantiomer through the membrane. Herein, the new electrospun membranes made of the CDMPCs synthesized from dried wood pulp was investigated for their enantioselective permeation properties. Enantioselective permeation properties of the CDMPCs membranes were characterized by liquid-liquid permeations of a racemic mixture, (*R*,*S*)-1-(1-naphthyl)ethanol, through the CDMPCs membranes that were sandwiched between commercially

available PTFE membrane filters as support materials using a pair of "Side-Bi-Side" glass cells as shown in Figure 8. A solution of the racemic mixture in the eluent (*n*-hexane/2-propanol = 9/1 (v/v)) was placed in the left-side cell and the same volume of pure eluent was placed in the right-side cell. Under gentle stirring, a portion of the solution in the right-side cell was sampled every 1 minute to determine *e.e.* (%) of a preferentially permeated enantiomer by the HPLC analysis. This procedure was performed for all the CDMPCs membranes and their enantioselective permeation properties were investigated based on their *e.e.* versus permeation time. As expected, the *S*-enantiomer was preferentially permeated through all the CDMPCs membranes by the liquid-liquid permeation. The *e.e.* values of the *S*-enantiomer in the right-side cell were plotted against the time and shown in Figure 9a and 9b for the permeations using the membranes made of CDMPC-10 (Membrane 1-3) and CDMPC-200 (Membrane 4 and 5), respectively. In case of the permeations through Membrane-2 (red line in Figure 9a) and Membrane-4 (pink line in Figure 9b), the highest *e.e.* values were observed at 1 min, then the *e.e.* values were gradually decreased over time. These results are in line with the previous result for the liquid-liquid permeation through the membrane made of CDMPC-MCC. As we previously reported for the CDMPC-MCC membrane, these gradual decreases of the *e.e.* values from the initial stage indicates that the enantioselective sorption of the *R*-enantiomer in these CDMPCs membranes reached equilibrium at 1 min or before, then both the *R*- and *S*-enantiomers permeate equally through the membranes, resulting in the gradual decrease of the *e.e.* values over time. On the other hand, the permeations through Membrane-1 (black line in Figure 9a), Membrane-3 (blue line in Figure 9a), and Membrane-5 (green line in Figure 9b) demonstrated different behavior, i.e., the *e.e.* values gradually increased to the highest values and then decreased. These results probably suggest that the enantioselective sorption of the *R*-enantiomer in these CDMPCs membranes did not reach equilibrium at the initial stage until the time at which the *e.e.* values became maximum. Such a difference in the permeation behavior of the membranes can be attributed to a complex interplay of the parameters, such as thickness, SSA, and surface energy of the membranes as summarized in Table 2. Further study on controlling these parameters is necessary to investigate the sorption capacity of the membranes.

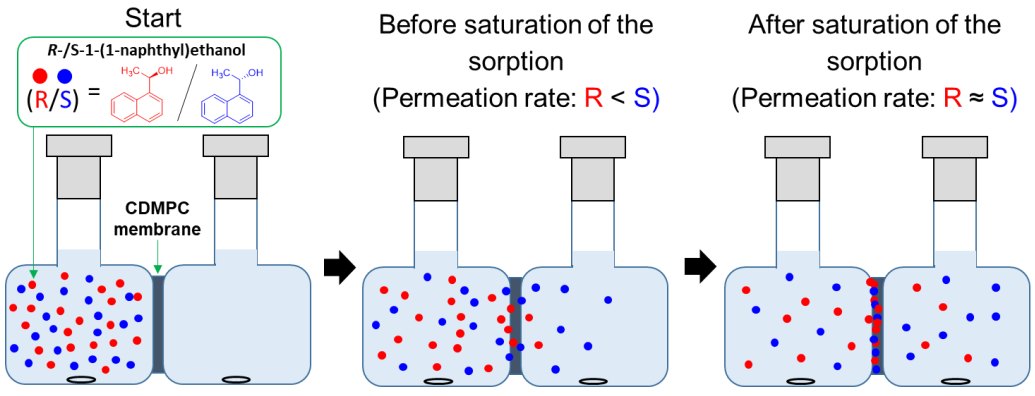

Figure 8. Schematic illustration of the LLP experiment.

In addition to the experimental approach described above, theoretical approaches such as molecular modeling is of great importance to elucidate the mechanism of chiral recognition within the CDMPCs membranes. Herein, the energy and geometry of the interactions of CDMPC with *R*-

and *S*-1-(1-naphthyl)ethanol were studied by molecular docking simulations using AutoDock molecular modeling simulation software. Previous studies have shown that the chiral recognition sites of CDMPC exist in the cavities between the sheets formed by the cellulose backbone, which incorporate various levels of chiral information (Adhikari et al. 2023; Kasat et al. 2007; Peluso et al. 2019). Discriminations of chiral molecules originate in the fit between such chiral cavities and the enantiomers that is affected by diverse interactions during the separation process (Scriba 2016). The binding free energy (ΔG) which evaluates the thermodynamic stability of the complex of CDMPC and *R-/S*-1-(1-naphthyl)ethanol was calculated by a semi-empirical binding free energy function in the AutoDock. The results of docking simulations are shown in Figure 10 and the calculated ΔG values are listed in Table 3. The obtained ΔG values for both the *R*- and *S*-enantiomers were negative, indicating that the retentions of *R*- and *S*-1-(1-naphthyl)ethanol in the cavities of CDMPC are enthalpy driven and spontaneous processes (Li et al. 2010; Yao et al. 2017). In addition, the higher negative ΔG value for the *R*-enantiomer (ΔG = -4.732 kcal/mol) than that for *S*-enantiomer (ΔG = -4.687 kcal/mol) indicates stronger retention of the *R*-enantiomer than the *S*-enantiomer. In Figure 10a, the 3D docking pose of the *R*-1-(1-naphthyl)ethanol and CDMPC demonstrates that the naphthalene group in the *R*-enantiomer (shown in green) aligns "in phase" with the phenyl ring in CDMPC. On the other hand, the naphthalene group in the *S*-enantiomer (shown in pink) aligns slightly out of phase with the phenyl ring in CDMPC as shown in Figure 10b. This is supported by the shorter π–π interactions distances between the *R*-enantiomer and CDMPC as reported in Table 3, confirming that there exist stronger π–π interactions between CDMPC and the *R*-enantiomer than the *S*-enantiomer. Furthermore, the distances of the hydrogen bondings formed between the urethane groups of CDMPC and the hydroxyl group of the *R*-enantiomer (2.05 Å and 2.48 Å as shown in Figure 10c) are shorter than those of the *S*-enantiomer (2.12 Å and 2.69 Å as shown in Figure 10d), suggesting stronger interaction of CDMPC with the *R*-enantiomer. These results indicate that the enantioselective permeation of *S*-1-(1-naphthyl)ethanol through the CDMPCs membranes is based-on a stronger interaction and higher binding energy between the *R*-enantiomer and CDMPC (the difference in binding energy |ΔΔG| between the *R*- and *S*-enantiomers is 0.046 kcal/mol).

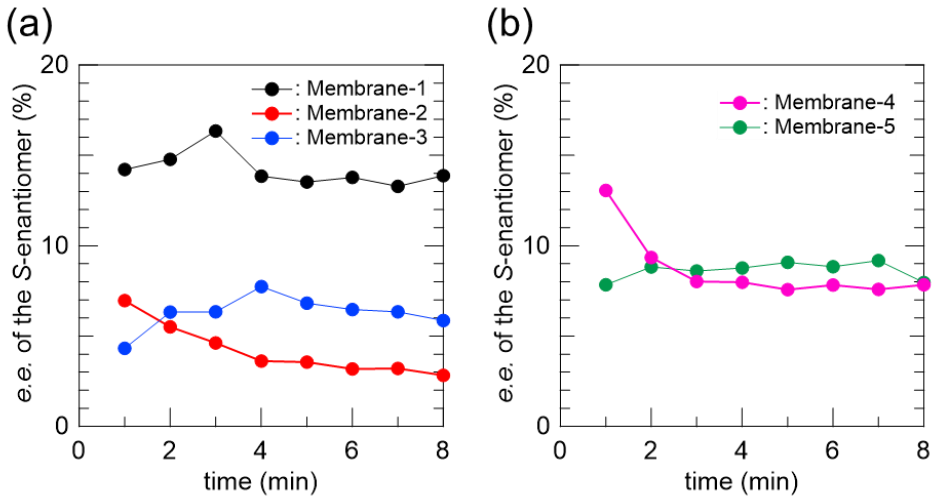

Figure 9. Plots of *e.e.* (%) of the preferentially permeated *S*-enantiomer though the electrospun membranes from (a) the solutions of CDMPC-10 and (b) those of CDMPC-200 vs time of the permeation.

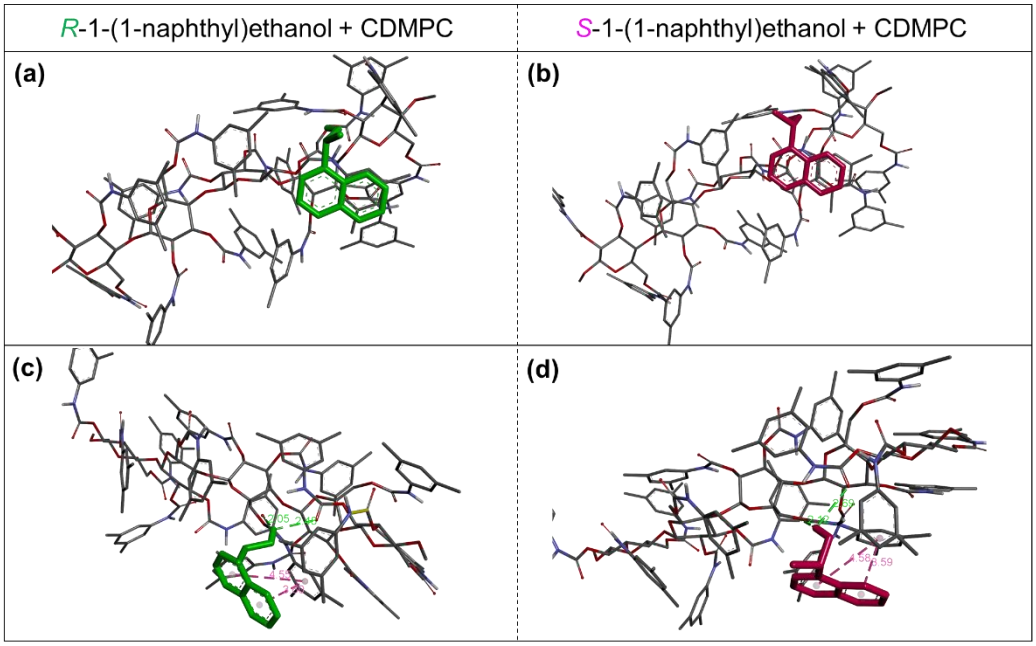

Figure 10. The 3D docking pose of enantiomers of (a and c) *R*- and (b and d) *S*-1-(1-naphthyl)ethanol with CDMPC.

Table 3. Binding free energies and interactions between CDMPC and *R*-/*S*-1-(1-naphthyl)ethanol calculated by molecular docking method

Chiral molecule	ΔG (kcal/mol)	|ΔΔG|[a] (kcal/mol)	Number of π–π interactions (distances in Å)	Number of hydrogen bondings (distances in Å)
R-1-(1-naphthyl)ethanol	-4.732	0.046	2 (3.60/4.55)	2 (2.05/2.48)
S-1-(1-naphthyl)ethanol	-4.687		2 (3.59/4.58)	2 (2.12/2.69)

[a] Absolute value of difference of free binding energy between the *R*- and *S*-enantiomer.

Conclusions

In summary, commercially available hardwood cellulose fiber samples having different fiber length (TECHNOCEL-10, -200, and -1000) were successfully functionalized to obtain CDMPCs having different DPs (CDMPC-10, -200, and -1000). The CDMPCs were electrospun with specific parameters (solvent, solution feed rate, applied voltage) to form continuous nanofibers and their nonwoven membranes. The morphology of the fibers and membranes were affected by the DP and the concentration of the CDMPCs, i.e. overall, the mean diameter of the fibers tended to increase with the DP and the concentration. The liquid-liquid permeation of (*R*,*S*)-1-(1-naphthyl)ethanol through the five examples of the CDMPCs membranes all demonstrated preferable permeations of the *S*-enantiomer. The theoretical molecular docking simulations of CDMPC with *R*- and *S*-1-(1-naphthyl)ethanol indicated the enantioselective permeation is due to better retention of the *R*-enantiomer in the chiral recognition cites of CDMPC with higher binding energy via hydrogen bonding and π–π interactions. These findings are a good step forward toward novel chiral resolution system using electrospun nanofibrous membranes consisting of various CSs already used for chiral HPLC.

Acknowledgments

The authors thank Ms. P. Chaud for the SSA measurements, Ms. S. Ortega Murillo for the WCA measurements, Dr. C. Lancelon-Pin for the SEM observation at the Electronic Microscopy Platform (PMIEL) of the Institut de Chimie Moléculaire de Grenoble (ICMG), and Ms. L. Buon and Mr. E. Bayma for the HPLC analysis at the Chromatography and Sugar Analysis Platform (PCANS) of the CERMAV. The authors are thankful to Drs. K. Mazeau, Y. Nishiyama, and J.-L.

Putaux (CERMAV) for fruitful discussions and to Prof. R. Pecora (Stanford University) for helpful suggestions during the writing of this manuscript.

Authors' contributions

The manuscript was written through contributions of all authors. / All authors have given approval to the final version of the manuscript.

Funding

This study was financially supported by the Institut Carnot PolyNat (ANR-16-CARN-0025-0), the Centre de Recherches sur les Macromolécules Végétales (CERMAV, CNRS), Université Grenoble Alpes ARCANE Bio-driven chemistry and CBH-EUR-GS (ANR-17-EURE-0003).

Availability of data and materials

Not applicable.

Declarations

Conflict of interests

The authors declare that they have no competing interests.

Ethics approval and consent to participate

Not applicable.

Consent for publication

Not applicable.

References

Adhikari S, Bhujbal S, Paik M-J, Lee W (2023) Enantioseparation and molecular modeling study of chiral amines as three naphthaldimine derivatives using amylose or cellulose trisphenylcarbamate chiral stationary phases Chirality 35:29-39 doi:https://doi.org/10.1002/chir.23513

Ahmadi-Nohadani H, Nono-Tagne S, Barrett CJ, Otsuka I (2022) Electrospun Azo-Cellulose Fabric: A Smart Polysaccharidic Photo-Actuator Macromol Rapid Commun 43:e2200063 doi:https://doi.org/10.1002/marc.202200063

Brunauer S, Emmett PH, Teller E (1938) Adsorption of Gases in Multimolecular Layers Journal of the American Chemical Society 60:309-319 doi:https://doi.org/10.1021/ja01269a023

Bui CV, Rosenau T, Hettegger H (2023) Synthesis by carbonate aminolysis and chiral recognition ability of cellulose 2,3-bis(3,5-dimethylphenyl carbamate)-6-(α-phenylethyl carbamate) selectors Cellulose 30:153-168 doi:https://doi.org/10.1007/s10570-022-04898-8

Das S, Xu S, Ben T, Qiu S (2018) Chiral Recognition and Separation by Chirality-Enriched Metal–Organic Frameworks Angewandte Chemie International Edition 57:8629-8633 doi:https://doi.org/10.1002/anie.201804383

Fong H, Chun I, Reneker DH (1999) Beaded nanofibers formed during electrospinning Polymer 40:4585-4592 doi:https://doi.org/10.1016/S0032-3861(99)00068-3

Fumagalli M, Ouhab D, Boisseau SM, Heux L (2013) Versatile Gas-Phase Reactions for Surface to Bulk Esterification of Cellulose Microfibrils Aerogels Biomacromolecules 14:3246-3255 doi:https://doi.org/10.1021/bm400864z

Gong W, Chen Z, Dong J, Liu Y, Cui Y (2022) Chiral Metal–Organic Frameworks Chemical Reviews 122:9078-9144 doi:https://doi.org/10.1021/acs.chemrev.1c00740

Greiner A, Wendorff JH (2007) Electrospinning: a fascinating method for the preparation of ultrathin fibers Angew Chem, Int Ed 46:5670-5703 doi:https://doi.org/10.1002/anie.200604646

Kasat RB, Wang N-HL, Franses EI (2007) Effects of Backbone and Side Chain on the Molecular Environments of Chiral Cavities in Polysaccharide-Based Biopolymers Biomacromolecules 8:1676-1685 doi: https://doi.org/10.1021/bm070006h

Kawasaki T, Yoshikawa M (2013) Nanofiber membranes from cellulose triacetate for chiral separation Desalination and Water Treatment 51:5080-5088 doi:https://doi.org/10.1080/19443994.2013.768832

Kaya C, Birgül K, Bülbül B (2023) Fundamentals of chirality, resolution, and enantiopure molecule synthesis methods Chirality 35:4-28 doi:https://doi.org/10.1002/chir.23512

Ke J, Yang K, Bai X, Luo H, Ji Y, Chen J (2021) A novel chiral polyester composite membrane: Preparation, enantioseparation of chiral drugs and molecular modeling evaluation Separation and Purification Technology 255:117717 doi:https://doi.org/10.1016/j.seppur.2020.117717

Lee H, Nishino M, Sohn D, Lee JS, Kim IS (2018) Control of the morphology of cellulose acetate nanofibers via electrospinning Cellulose 25:2829-2837 doi:https://doi.org/10.1007/s10570-018-1744-0

Li Y, Liu D, Wang P, Zhou Z (2010) Computational study of enantioseparation by amylose tris(3,5-dimethylphenylcarbamate)-based chiral stationary phase Journal of Separation Science 33:3245-3255 doi:https://doi.org/10.1002/jssc.201000266

Liu T, Li Z, Wang J, Chen J, Guan M, Qiu H (2021) Solid membranes for chiral separation: A review Chemical Engineering Journal 410:128247 doi:https://doi.org/10.1016/j.cej.2020.128247

Luo H, Bai X, Liu H, Qiu X, Chen J, Ji Y (2022) β-Cyclodextrin covalent organic framework modified-cellulose acetate membranes for enantioseparation of chiral drugs Separation and Purification Technology 285:120336 doi:https://doi.org/10.1016/j.seppur.2021.120336

Mizushima H, Yoshikawa M, Li N, Robertson GP, Guiver MD (2012) Electrospun nanofiber membranes from polysulfones with chiral selector aimed for optical resolution European Polymer Journal 48:1717-1725 doi:https://doi.org/10.1016/j.eurpolymj.2012.07.003

Motamedi AS, Mirzadeh H, Hajiesmaeilbaigi F, Bagheri-Khoulenjani S, Shokrgozar M (2017) Effect of electrospinning parameters on morphological properties of PVDF nanofibrous scaffolds Progress in Biomaterials 6:113-123 doi:https://doi.org/10.1007/s40204-017-0071-0

Okamoto Y, Ikai T (2008) Chiral HPLC for efficient resolution of enantiomers Chemical Society Reviews 37:2593-2608 doi:https://doi.org/10.1039/B808881K

Okamoto Y, Kawashima M, Hatada K (1986) Chromatographic resolution: XI. Controlled chiral recognition of cellulose triphenylcarbamate derivatives supported on silica gel Journal of Chromatography A 363:173-186 doi:https://doi.org/10.1016/S0021-9673(01)83736-5

Okamoto Y, Yashima E (1998) Polysaccharide Derivatives for Chromatographic Separation of Enantiomers Angewandte Chemie International Edition 37:1020-1043 doi:https://doi.org/10.1002/(SICI)1521-3773(19980504)37:8<1020::AID-ANIE1020>3.0.CO;2-5

Otsuka I, Pandey K, Ahmadi-Nohadani H, Nono-Tagne S (2021) Electrospun Cellulosic Membranes toward Efficient Chiral Resolutions via Enantioselective Permeation ACS Macro Letters 10:921-925 doi:https://doi.org/10.1021/acsmacrolett.1c00349

Peluso P, Dessì A, Dallocchio R, Mamane V, Cossu S (2019) Recent studies of docking and molecular dynamics simulation for liquid-phase enantioseparations ELECTROPHORESIS 40:1881-1896 doi:https://doi.org/10.1002/elps.201800493

Peluso P, Mamane V, Dallocchio R, Dessì A, Cossu S (2020) Noncovalent interactions in high-performance liquid chromatography enantioseparations on polysaccharide-based chiral selectors Journal of Chromatography A 1623:461202 doi:https://doi.org/10.1016/j.chroma.2020.461202

Scriba GKE (2016) Chiral recognition in separation science – an update Journal of Chromatography A 1467:56-78 doi:https://doi.org/10.1016/j.chroma.2016.05.061

Shen J, Okamoto Y (2016) Efficient Separation of Enantiomers Using Stereoregular Chiral Polymers Chemical Reviews 116:1094-1138 doi:https://doi.org/10.1021/acs.chemrev.5b00317

Shiomi K, Yoshikawa M (2013) Multi-stage chiral separation with electrospun chitin nanofiber membranes Separation and Purification Technology 118:300-304 doi:https://doi.org/10.1016/j.seppur.2013.07.004

Shiomi K, Yoshikawa M (2016) Molecularly imprinted chitin nanofiber membranes: multi-stage cascade membrane separation within the membrane J Membr Sep Technol 5:103-114 doi:https://doi.org/10.6000/1929-6037.2016.05.03.3

Sueyoshi Y, Utsunomiya A, Yoshikawa M, Robertson GP, Guiver MD (2012) Chiral separation with molecularly imprinted polysulfone-aldehyde derivatized nanofiber membranes☆ Journal of Membrane Science 401-402:89-96 doi:https://doi.org/10.1016/j.memsci.2012.01.033

Thompson CJ, Chase GG, Yarin AL, Reneker DH (2007) Effects of parameters on nanofiber diameter determined from electrospinning model Polymer 48:6913-6922 doi:https://doi.org/10.1016/j.polymer.2007.09.017

Vedovello P, Marcio Paranhos C, Fernandes C, Elizabeth Tiritan M (2022) Chiral polymeric membranes: Recent applications and trends Separation and Purification Technology 280:119800 doi:https://doi.org/10.1016/j.seppur.2021.119800

Wang Z, Zhang S, Chen Y, Zhang Z, Ma S (2020) Covalent organic frameworks for separation applications Chemical Society Reviews 49:708-735 doi:https://doi.org/10.1039/C9CS00827F

Weng X et al. (2013) Synthesis and characterization of cellulose 3,5-dimethylphenylcarbamate silica hybrid spheres for enantioseparation of chiral β-blockers Journal of Chromatography A 1321:38-47 doi:https://doi.org/10.1016/j.chroma.2013.10.048

Yao Y, Song P, Wen X, Deng M, Wang J, Guo X (2017) Chiral separation of 12 pairs of enantiomers by capillary electrophoresis using heptakis-(2,3-diacetyl-6-sulfato)-β-cyclodextrin as the chiral selector and the elucidation of the chiral recognition mechanism by computational methods Journal of Separation Science 40:2999-3007 doi:https://doi.org/10.1002/jssc.201700137

Yoshikawa M, Nakai K, Matsumoto H, Tanioka A, Guiver MD, Robertson GP (2007) Molecularly Imprinted Nanofiber Membranes from Carboxylated Polysulfone by Electrospray Deposition Macromolecular Rapid Communications 28:2100-2105 doi:https://doi.org/10.1002/marc.200700359

Yoshimatsu K, Ye L, Lindberg J, Chronakis IS (2008) Selective molecular adsorption using electrospun nanofiber affinity membranes Biosensors and Bioelectronics 23:1208-1215 doi:https://doi.org/10.1016/j.bios.2007.12.002

Zhuo S, Zhang X, Luo H, Wang X, Ji Y (2020) The Application of Covalent Organic Frameworks for Chiral Chemistry Macromolecular Rapid Communications 41:2000404 doi:https://doi.org/10.1002/marc.202000404